Electronic Supplementary Material (ESI) for Dalton Transactions.

Engineering $NiMoO_4$/NiFe LDH/rGO Multicomponent Nanosheets toward Enhanced Electrocatalytic Oxygen Evolution Reaction

Lei Jin, Qing Wang, Kun Wang, Yuchen Lu, Bingji Huang, Hui Xu*, Xingyue Qian, Lida Yang, Guangyu He*, Haiqun Chen*

Key Laboratory of Advanced Catalytic Materials and Technology, Advanced Catalysis and Green Manufacturing Collaborative Innovation Center, Changzhou University, Changzhou, Jiangsu Province 213164, China.

Corresponding authors: xuhui006@cczu.edu.cn (H. Xu); hegy@cczu.edu.cn (G. He); hqchen@ccdu.edu.cn (H. Chen)

Materials and methods

1.Reagents

All chemicals utilized in the present work were purchased from Sinopharm Chemical Reagent Co, Ltd (China), including nickel nitrate hexahydrate $Ni(NO_3)_2 \cdot 6H_2O$, iron nitrate nonahydrate ($Fe(NO_3)_3 \cdot 9H_2O$), sodium molydbate dehydrate ($Na_2MoO_4 \cdot 2H_2O$), urea ($CO(NH_2)_2$), ethanol (C_2H_5OH) and potassium hydroxide (KOH). All of the above chemicals were of analytical grade and used as received without further purification.

2.Preparations

Graphite oxide (GO) was prepared from scaly graphite powder through Hummers' method.[25]

2.1 Synthesis of $NiMoO_4$ nanosheets

The pristine $NiMoO_4$ nanosheets were synthesized by a hydrothermal method. Typically, $Ni(NO_3)_2.6H_2O$ (4 mmol), $Na_2MoO_4 \cdot 2H_2O$ (4 mmol), and $CO(NH_2)_2$ (15 mmol) were dissolved in 50 mL of distilled water under sonication conditions, after stirring for 30 min, the solution was transferred to a 100 mL Teflon-lined stainless-steel autoclave, which was sealed and maintained at 150°C for 6 h. After cooling to room temperature naturally, the solid green produce was washed with deionized water and vacuum-dried at 60°C.

2.2 Synthesis of $NiMoO_4$/NiFe LDH

$Ni(NO_3)_2 \cdot 6H_2O$ (0.1 mmol), $Fe(NO_3)_3 \cdot 9H_2O$ (0.1 mmol), and $CO(NH_2)_2$ (5 mmol) were dissolved in 50 mL of distilled water to form a clear solution after 20 min of reaction with sonication. Next, the freshly prepared $NiMoO_4$ (0.4 mmol) nanosheets that dispersed into 10 mL deionized water was dropped into above solution. After drastically stirring for 30 min at room temperature, the solution was transferred to a 100 mL Teflon-lined stainless-steel autoclave and maintained at

120°C for 12 h. Finally, the yellow solid products were collected and dried, the synthetic product was named as $NiMoO_4$/NiFe LDH.

2.3 Synthesis of $NiMoO_4$/NiFe LDH/rGO

$NiMoO_4$/NiFe LDH/rGO_x composites with different contents of rGO (x = 5, 10 and 15 wt%) were synthesized by a hydrothermal method. In a typical procedure for preparing $NiMoO_4$/NiFe LDH/$rGO_{10\%}$, 4.17 mL of GO suspension (0.272 wt%), $Ni(NO_3)_2{\cdot}6H_2O$ (0.1 mmol), $Fe(NO_3)_3{\cdot}9H_2O$ (0.1 mmol), and $CO(NH_2)_2$ (5 mmol) were dissolved in 46 mL of distilled water to form a clear solution after 3 h of reaction with sonication, Next, the $NiMoO_4$ (0.4 mmol) nanosheets that dispersed into 10 mL deionized water was dropped into above solution, After drastic stirring for 30 min at room temperature, the solution was transferred to a 100 mL Teflon-lined stainless steel autoclave and maintained at 120°C for 12 h. After cooling to room temperature naturally, the black solid produce was washed and vacuum-dried at 60°C. For comparison, NiFe LDH was prepared in the absence of GO and $NiMoO_4$ while keeping other reaction with the same conditions.

3.Material characterizations

The crystal phases and structures of the as-prepared samples were characterized by powder X-ray diffraction (XRD) with Bruker D8 Advance diffractometer (Cu Ka radiation, λ = 0.15418 nm) in the 2θ range of 10-80° at a scanning rate of 0.05° s^{-1}. The microstructures of the products were observed by transmission electron microscopy (TEM, JEM-2100F) and field-emission scanning electron microscopy (FESEM, Zeiss Supra 55) that equipped with element mappings and energy dispersive spectrometry (EDS). Raman spectra (Japan LabRAMHR evolution) of samples were recorded on a Renishaw in ViaReflex Raman microprobe. X-ray photoelectron spectroscopy (XPS,

PHI-5000C ESCA, PerkinElmer, USA) was employed to obtain elemental information of prepared catalysts on a VG ESCALAB MKII using Al Ka radiation. The N_2 adsorption desorption isotherms and the pore size distributions were characterized by Brunauer-Emmett-Teller method (BET, ASAP2010C).

4. Electrochemical measurements

All the electrochemical measurements were operated using a CHI760 electrochemical workstation with a standard three electrode cell. The reference and counter electrodes were Hg/HgO and graphite rod, respectively. A glassy carbon electrode (GCE, 0.196 cm^2 area) that modified with catalyst ink is used as the working electrode. For the preparation of the catalyst ink, 2 mg of catalyst and 20 μL Nafion (5 wt%) was dissolved in 360 μL ethanol and 120 μL H_2O, the ink was sonicated for 2 h to enable the solution to be uniformly dispersed. Then, 10 μL of the catalyst ink was dropped on the surface of GCE with a mass loading of 203.8 $\mu g \cdot cm^{-2}$. All potentials were measured against Hg/HgO and converted to reversible hydrogen electrode (RHE) by Nernst equation: $E_{vs\ RHE} = E_{vs\ Hg/HgO} + 0.0591\ pH + 0.098$. The overpotential (η) was calculated through the formula: $\eta = E_{RHE} - 1.23$ V. Cyclic Voltammograms (CV) were measured at a scan rate of 5 $mV \cdot s^{-1}$, Electrochemical impedance spectroscopy was tested over the frequency range of 10^6 to 10^{-2} Hz with an AC signal amplitude of 5 mV. The double-layer capacitances (C_{dl}) were calculated through CV at different scan rates (*i.e.* 20, 40, 60, 80 and 100 $mV \cdot s^{-1}$) in 1.0 M KOH, which was used to evaluate the electrochemical active surface areas (ECSA). The long-term stability of the catalyst was conducted by chronopotentiometry. All the data of electrochemistry were presented without any iR correction.

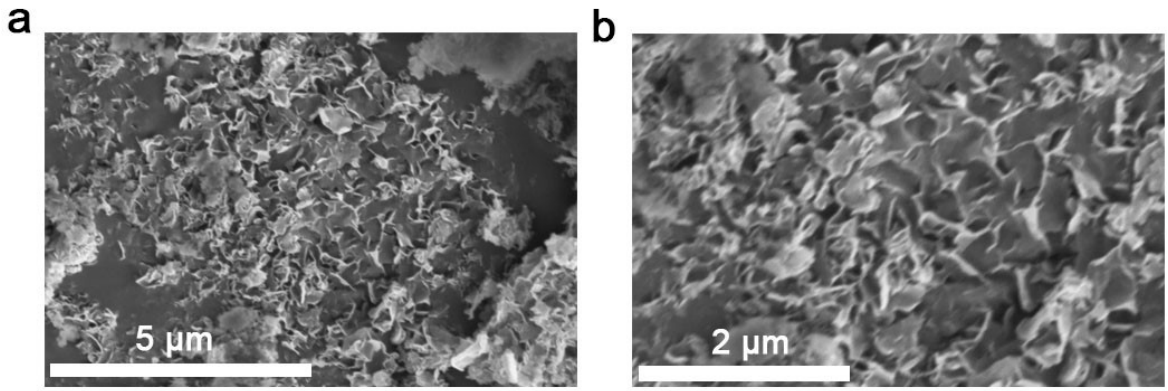

Fig.S1 (a, b) SEM images of $NiMoO_4$.

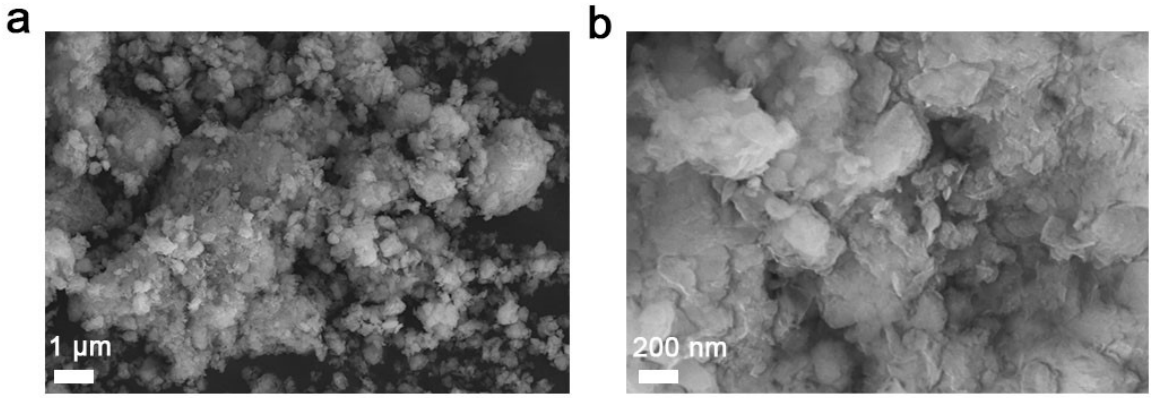

Fig.S2 (a, b) SEM images of $NiMoO_4$/NiFe LDH.

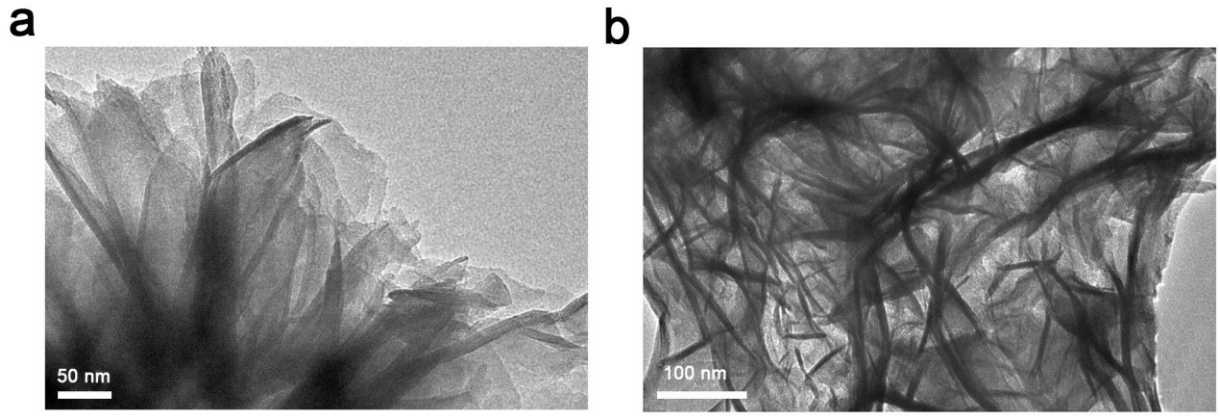

Fig.S3 (a, b) TEM images of $NiMoO_4$/NiFe LDH/$rGO_{10\%}$

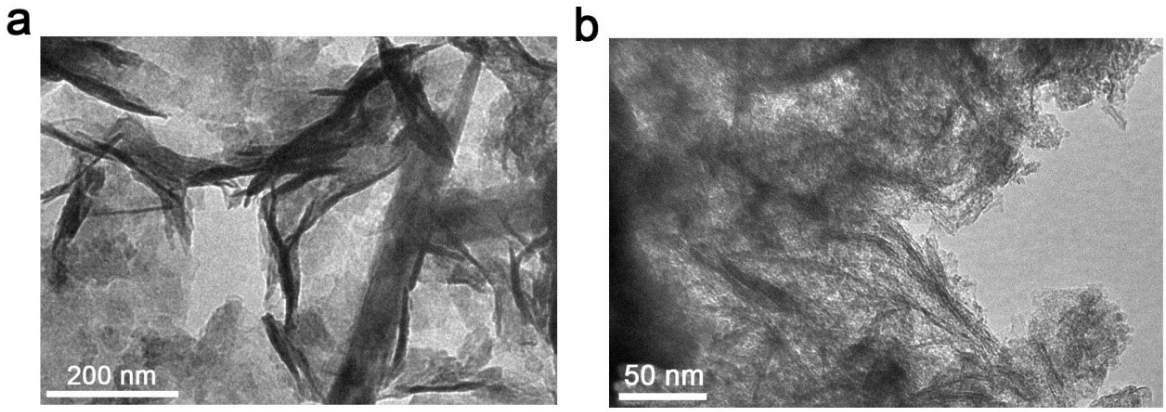

Fig.S4 (a, b) TEM images of $NiMoO_4$ and NiFe LDH.

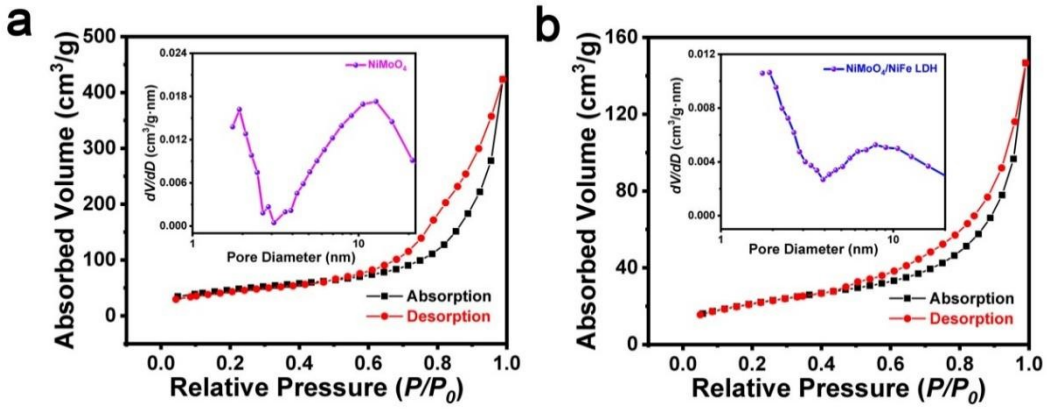

Fig.S5 N_2 adsorption desorption isotherm of (a) $NiMoO_4$ and (b) $NiMoO_4$/NiFe LDH.

Table S1 BET surface area of $NiMoO_4$, NiFe LDH, $NiMoO_4$/NiFe LDH and $NiMoO_4$/NiFe LDH/$rGO_{10\%}$ composites.

Samples	BET Surface area ($m^2 \cdot g^{-1}$)
$NiMoO_4$	164.5
NiFe LDH	74.5
$NiMoO_4$/NiFe LDH	75.7
$NiMoO_4$/NiFe LDH/$rGO_{10\%}$	101.8

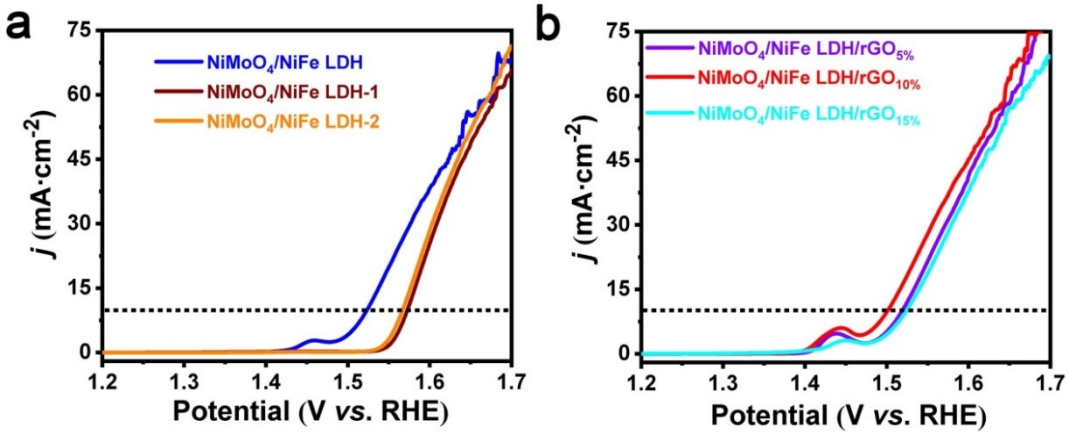

Fig.S6 (a) LSV curves of $NiMoO_4$/NiFe LDH, $NiMoO_4$/NiFe LDH-x (x=1, 2) and (b) $NiMoO_4$/NiFe LDH/rGO_x (x= 5%, 10% and 15%).

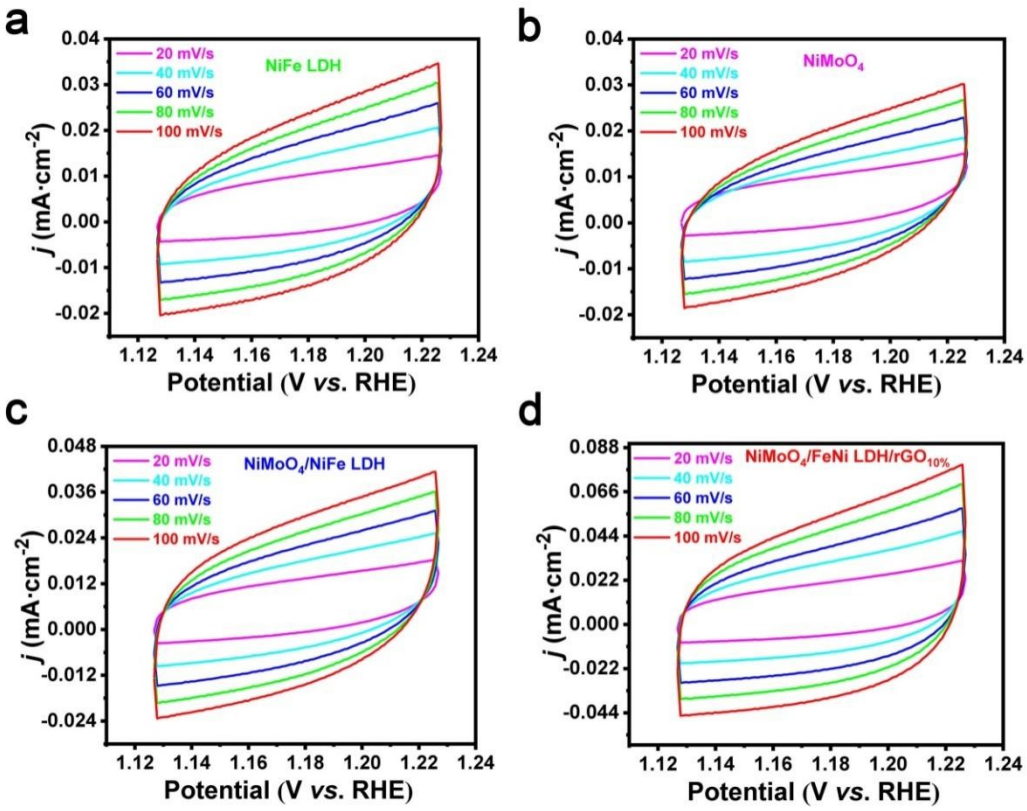

Fig.S7 (a) CV curves of NiFe LDH, (b) $NiMoO_4$, (c) $NiMoO_4$/NiFe LDH and (d) $NiMoO_4$/NiFe LDH/$rGO_{10\%}$.

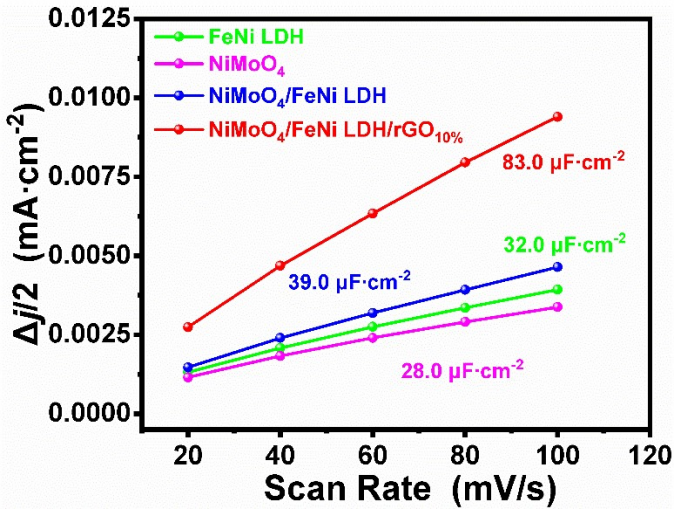

Fig.S8 Double layer currents of different catalysts versus scan rate.

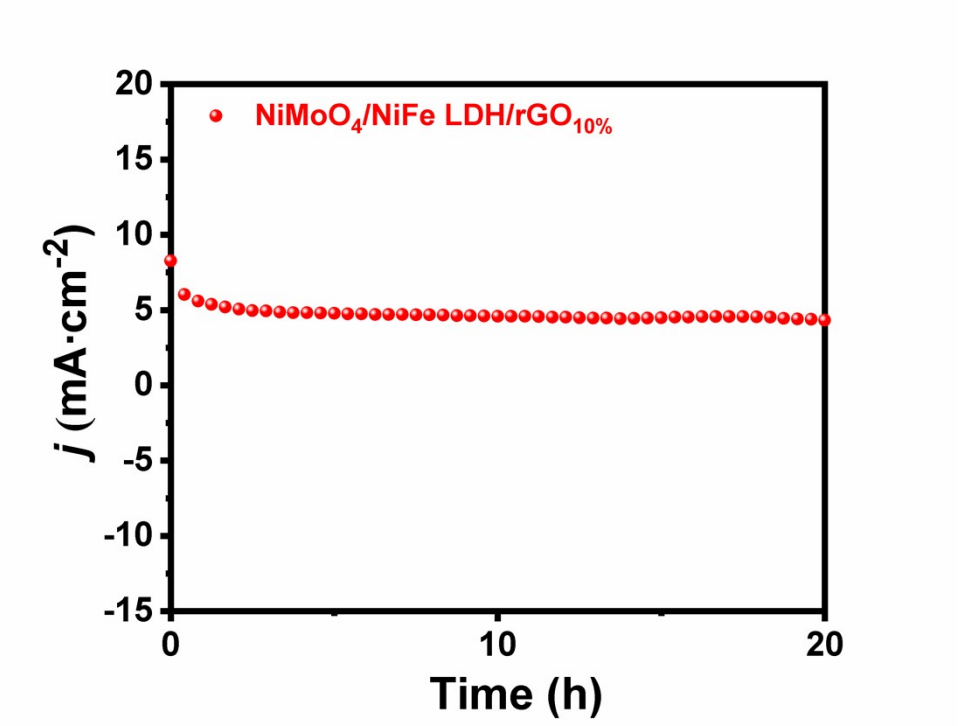

Fig.S9 Chronoamperometric curve of $NiMoO_4$/NiFe LDH/$rGO_{10\%}$ at a voltage of 1.5 V (vs. RHE).

Table S2 OER activity comparison of different catalysts in alkaline condition (η: overpotential at the current density of 10 mA·cm^{-2}).

Catalysts	electrolyte	η(mV)	Tafel slope (mV/dec)	Reference
$NiMoO_4$@NiFe LDH-$r_{10\%}$	**1.0 M KOH**	**270**	**78.2**	**This Work**
$NiMoO_4$NRs-Fe-1	1.0 M KOH	351	69	[1]
$FeZn_4Co$@CNFs	0.1 M KOH	360	69	[2]
Co/Ni@GC/NCNTs/CNFs	1.0 M KOH	395	64	[3]
$Zn_{0.4}Ni_{0.6}Co_2O_4$/NCNTs	0.1 M KOH	410	118	[4]
FeNi/$(FeNi)_9S_8$	1.0 M KOH	283	64	[5]
Fe_2M-MIL-88B	0.1 M KOH	307	38	[6]
ODAC-CoO	0.1 M KOH	364	68.6	[7]
$Sr2Co_{1.5}Fe_{0.5}O_{6-\delta}$	1.0 M KOH	318	44.8	[8]
FeNi-LDH/Ti_3C_2	1.0 M KOH	298	43	[9]
NiMn-LDH-rGO	1.0 M KOH	280	46	[10]
FeNi-LDH/3D carbon	0.1 M KOH	340	71	[11]
ER-Co_3O_4NWs-2	1.0 M KOH	370	70	[12]
CoO–MoO_2	1.0 M KOH	312	70	[13]
NiMo-FG	1.0 M KOH	338	67	[14]
$CoFe_2O_4$	1.0 M KOH	275	42	[15]
$Co_2Mo_3O_8$@NC-800	1.0 M KOH	331	88	[16]

References

[1] C. Ye, J. Liu, Q. Zhang, X. Jin, Y. Zhao, Z. Pan, G. Chen, Y. Qiu, D. Ye, L. Gu, *J. Am. Chem. Soc.* 2021, 143, 14169-14177.

[2] F. Wang, Z. Xiao, X. Liu, J. Ren, T. Xing, Z. Li, X. Li, Y. Chen, *J. Power Sources.* 2022, 521, 230925.

[3] J. Li, J. Qian, X. Chen, X. Zeng, L. Li, B. Ouyang, E. Kan, W. Zhang, *Comp. Part B: Eng.* 2021, 231 109573.

[4] X.T. Wang, T. Ouyang, L. Wang, J.H. Zhong, Z.Q. Liu, *Angew. Chem. Int. Ed.* 2020, 132, 132 6554-6561.

[5] H.-L. Meng, S.-Y. Lin, J.-J. Feng, L. Zhang, A.-J. Wang, *J. Colloid Interface Sci.* 2022, 610, 573-582.

[6] C. Wu, X. Zhang, H. Li, Z. Xia, S. Yu, S. Wang, G. Sun, Chin. *J. Catal.* 2021, 42, 637-647.

[7] Y. Tian, X. Liu, L. Xu, D. Yuan, Y. Dou, J. Qiu, H. Li, J. Ma, Y. Wang, D. Su, *Adv. Funct. Mater.* 2021, 31, 2101239.

[8] S.R. Ede, C.N. Collins, C.D. Posada, G. George, H. Wu, W.D. Ratcliff, Y. Lin, J. Wen, S. Han, Z. Luo, *ACS Catal.* 2021, 11, 4327-4337.

[9] M. Yu, S. Zhou, Z. Wang, J. Zhao, J. Qiu, *Nano Energy* 2018, 44, 181-190.

[10] W. Ma, R. Ma, J. Wu, P. Sun, X. Liu, K. Zhou, T. Sasaki, *Nanoscale* 2016, 8, 10425-10432.

[11] W. Wang, Y. Liu, J. Li, J. Luo, L. Fu, S. Chen, *J. Mater. Chem. A* 2018, 6, 14299-14306.

[12] S. Liu, H. Cheng, K. Xu, H. Ding, J. Zhou, B. Liu, W. Chu, C. Wu, Y. Xie, *ACS Energy Lett.* 2018, 4, 423-429.

[13] F. Lyu, Y. Bai, Z. Li, W. Xu, Q. Wang, J. Mao, L. Wang, X. Zhang, Y. Yin, *Adv. Funct. Mater.* 2017, 27, 1702324.

[14] S. Jeong, K. Hu, T. Ohto, Y. Nagata, H. Masuda, J.-i. Fujita, Y. Ito, *ACS Catal.* 2019, 10, 792-799.

[15] H. Fang, T. Huang, D. Liang, M. Qiu, Y. Sun, S. Yao, J. Yu, M.M. Dinesh, Z. Guo, Y. Xia, *J. Mater. Chem. A.* 2019, 7, 7328-7332.

[16] T. Ouyang, X.T. Wang, X.Q. Mai, A.N. Chen, Z.Y. Tang, Z.Q. Liu, *Angew. Chem. Int. Ed.* 2020, 59, 11948-11957.